

Measure, dimension, and complexity of escape in open Hamiltonian systems

Vitor M. de Oliveira, Matheus S. Palmero, and Iberê L. Caldas
Instituto de Física, Universidade de São Paulo, São Paulo, SP, Brazil

(Dated: March 15, 2022)

In this work, we introduce the *escape measure*, a finite-time version of the natural measure, to investigate the transient dynamics of escape orbits in open Hamiltonian systems. In order to numerically calculate the escape measure, we cover a region of interest of the phase space with a grid and we compute the visitation frequency of a given orbit on each box of the grid before the orbit escapes. Since open systems are not topologically transitive, we also define the *mean escape measure*, an average of the escape measure on an ensemble of initial conditions. We apply these concepts to study two physical systems: the single-null divertor tokamak, described by a two-dimensional map; and the Earth-Moon system, as modeled by the planar circular restricted three-body problem. First, by calculating the mean escape measure profile, we visually illustrate the paths taken by the escape orbits within the system. We observe that the choice of the ensemble of initial conditions may lead to distinct dynamical scenarios in both systems. Particularly, different orbits may experience different stickiness effects. After that, we analyze the mean escape measure distribution and we find that these vary greatly between the cases, highlighting the differences between our systems as well. Lastly, we define two parameters: the *escape correlation dimension*, that is independent of the grid resolution, and the *escape complexity coefficient*, which takes into account additional dynamical aspects, such as the orbit's escape time. We show that both of these parameters can quantify and distinguish between the diverse transient scenarios that arise.

I. INTRODUCTION

Near-integrable Hamiltonian systems are characterized by a rich dynamical setting with the usual presence of both chaotic and regular motion when the system is under a small perturbation [1]. In this case, its phase space is said to be *mixed* as it is composed by regions of stability along with a chaotic sea. In closed systems, chaotic orbits densely fill the chaotic area as the system is topologically transitive [2]. However, such motion is not uniform throughout the phase space and these orbits may temporarily concentrate in certain regions, a phenomenon called *stickiness* [3, 4].

In open Hamiltonian systems, on the other hand, the transitivity property does not hold and hence distinct chaotic orbits may describe very different paths before escaping [5]. In this situation, stickiness leads to *dynamical trapping* since the *escape orbits*, i.e., chaotic orbits that eventually exit the system, spend an expressive amount of time in sticky regions [3]. By opening a closed Hamiltonian system, the role of invariant manifolds as the geometrical structure behind the system's dynamics also becomes clear. For example, when there is more than one escape channel in the system, there exist fractal boundaries between the escape basins corresponding to each exit. These boundaries are formed by invariant manifolds associated with unstable periodic orbits [6].

In this work, we address the transient dynamics of open Hamiltonian systems and how it is affected by the choice of initial conditions. Specifically, we investigate how the paths described in the phase space by an ensemble of solutions prior to exiting the system differ from the paths taken by other ensembles. With this, we can assess which escape orbits experience dynamical effects such as stickiness and visually illustrate the influence of the system's

underlying geometrical structure. Such analysis is important for understanding the transient dynamics of various physical systems, especially in the fields of Plasma Physics and Celestial Mechanics, both of which are hallmarks of Hamiltonian mechanics [7–9].

Our analyzes are focused on two physical systems with different dynamical scenarios. The first one concerns the configuration of the magnetic field lines in a single-null divertor tokamak, which is described by a map with one degree of freedom. The second one concerns the motion of a body with negligible mass under the gravitational influence of the Earth and the Moon, as modeled by the two-degrees-of-freedom planar circular restricted three body problem. In both these systems, given our chosen parameters, we have a situation where there is only one exit and hence all escape orbits belong to the same escape basin.

To assist with our investigation, we define here a finite-time version of the natural measure specific for escape orbits: the *escape measure*. By calculating this measure for an ensemble of initial conditions, we depict the transient motion associated with such ensemble on a given area of the phase space. We later analyze the escape measure distribution for each chosen ensemble. Finally, in order to characterize each case, we define two parameters: the escape correlation dimension, which is similar to the correlation dimension; and the escape complexity coefficient, that attributes weights to the ensembles based on particular dynamical properties. Our results show that different scenarios may arise in the transient motion of the analyzed systems and that the escape measure is a powerful tool to visually illustrate and study these scenarios.

This paper is organized as follows. In Sec. II we define the concepts used in this work, namely, the escape

measure, the escape correlation dimension and the escape complexity coefficient. In Sec. III we apply these ideas to investigate the single-null divertor tokamak and the Earth-Moon system. Finally, we present our conclusions in Sec. IV.

II. MATHEMATICAL FRAMEWORK

A. Mean escape measure

Let $\varphi(\mathbf{x}_0, T)$ be a solution of our dynamical system with initial condition \mathbf{x}_0 and $t \in [0, T]$ and let us cover a region of the phase space that we are interested in by a grid of D -dimensional boxes of side-length ε . We call $\eta(B_i, \varphi(\mathbf{x}_0, T))$ the time spent by the orbit φ inside the box B_i .

If η is the same for almost every \mathbf{x}_0 , the *natural measure* for each box B_i can be defined as [10]

$$\mu_i = \lim_{T \rightarrow \infty} \frac{\eta(B_i, \varphi(\mathbf{x}_0, T))}{T}, \quad (1)$$

if the limit exists. It follows that $\sum_{i=1}^{N(\varepsilon)} \mu_i = 1$, where $N(\varepsilon)$ is the number of visited boxes, which depends on the box side-length ε .

The natural measure is defined in the asymptotic limit $T \rightarrow \infty$ and is usually associated with the dynamics of an orbit on a chaotic attractor. We are interested here, however, in the transient dynamics of escape orbits in open Hamiltonian systems. Then, we propose a finite-time version of Eq. (1), called the *escape measure*,

$$\mu_i^e = \frac{\eta(B_i, \varphi(\mathbf{x}_0, T^e))}{T^e}, \quad (2)$$

where T^e is the escape time, i.e., the time it takes for φ to reach a predefined escape region. It is important to note that $\sum_{i=1}^{N(\varepsilon)} \mu_i^e = 1$.

If we consider an orbit in the chaotic sea, the escape measure reflects the path followed by the orbit up until exiting the system. Hence, this measure is able to depict the transient dynamics of an escape orbit, including effects such as stickiness.

An observation here is in order. In practice, we use $\tilde{T}^e = \min(T^e, T_{max})$ instead of T^e in Eq. (2) since there is a computational time limit T_{max} for which we can numerically integrate an orbit and it can be shorter than the orbit's escape time. Evidently, if $T_{max} > T^e$, then $\tilde{T}^e = T^e$. This point will be addressed further later in this section.

Due to the lack of the transitivity property, a chaotic orbit of a open Hamiltonian system may escape before visiting all the available area on phase space. Therefore, in order to improve the statistics for later analysis and to better illustrate the behavior of escape orbits, we define the *mean escape measure*, the average of the escape measure on an ensemble U composed by M initial conditions,

$$\nu_i = \langle \mu_i^e \rangle_U = \frac{1}{M} \sum_{j=1}^M \mu_{i,j}^e, \quad (3)$$

where $\mu_{i,j}^e = \eta(B_i, \varphi(\mathbf{x}_{0,j}, T_j^e))/T_j^e$ is the escape measure for the j -th initial condition and box B_i . As before, we have that $\sum_{i=1}^N \nu_i = 1$.

Apart from the finite-time aspect, another difference of Eq. (2) from Eq. (1) is that we do not demand it holds for almost every \mathbf{x}_0 . With that, the mean escape measure, Eq. (3), is in fact a function of the ensemble of initial conditions:

$$\nu_i = \nu_i(U). \quad (4)$$

Hence, there are different transient behaviors in the system depending on the chosen set of initial conditions U , which can be illustrated by calculating the mean escape measure profile. Next, we present two approaches for quantifying Eq. (4).

B. Escape correlation dimension

The natural measure μ_i can also be seen as the visitation frequency on box B_i . In the context of dissipative dynamical systems, this measure shows which boxes are more visited by a typical orbit on a chaotic attractor. Associated with such attractor, then, a spectrum of generalized dimensions can be defined as [10]

$$D_q = \frac{1}{1-q} \lim_{\varepsilon \rightarrow 0} \frac{\ln I_q(\varepsilon)}{\ln(1/\varepsilon)}, \quad (5)$$

with

$$I_q(\varepsilon) = \sum_{i=1}^{N(\varepsilon)} \mu_i^q. \quad (6)$$

The main difference between the dimensions in Eq. (5) is given by Eq. (6), which attributes weight to the visitation frequency. Moreover, some D_q can be related to specific dynamical concepts. Here, we are interested in I_2 , which scales in the same fashion as the correlation integral in a time series [10, 11].

Similarly, we can define a spectrum of generalized dimensions associated with the mean escape measure, Eq. (3). However, instead of looking at the fractal geometry of an attractor, we are inspecting the paths taken by the escape orbits in an open Hamiltonian system. In special, we define the *escape correlation dimension*, which is given by

$$D_2^e = \lim_{\varepsilon \rightarrow 0} \frac{\ln I_2^e(\varepsilon)}{\ln \varepsilon}, \quad (7)$$

with

$$I_2^e(\varepsilon) = \sum_{i=1}^{N(\varepsilon)} \nu_i^2. \quad (8)$$

As the value of D_2 represents the degree to which the elements of an orbit are correlated, D_2^e returns a similar information, but for an ensemble of orbits. We then expect D_2^e to be high when there is stickiness in the system, for instance, which makes it a suitable quantity for analyzing the behavior of escape orbits.

For a D -dimensional phase space, we have that $D_2^e \leq D$. Numerically, we choose an ensemble U and calculate $I_2^e(\varepsilon)$ for different values of the box side-length ε . We then linearly interpolate these points in a log-log plot and determine the angular coefficient D_2^e .

C. Escape complexity coefficient

We now introduce another quantity for characterizing the dependency of the transient dynamics of escape orbits on the ensemble of initial conditions. Besides the visitation frequency, which is given by the mean escape measure, there are two other aspects that we can take into consideration for assessing the importance of a grid box.

First, the number of orbits m_i that begin in the ensemble U and pass through the box B_i is usually not the same for all boxes. Hence, we may say that the grid boxes with higher values of m_i have a higher influence on the ensemble and, consequently, on the system's escape properties.

Second, between the orbits that pass through a box B_i , the one with the largest escape time τ_i contributes the most to our analysis, since it reaches the highest number of box visitations. Therefore, we may consider a grid box more important if it has a higher τ_i .

We then define the *escape complexity coefficient* as

$$c = \sum_{i=1}^{N(\varepsilon)} \alpha_i \beta_i \nu_i, \quad (9)$$

where the weights of the boxes are given by

$$\alpha_i = \frac{m_i}{M} \quad \text{and} \quad \beta_i = \frac{\tau_i}{T_{max}}, \quad (10)$$

with M and T_{max} , as introduced before, the number of initial conditions and the maximum integration time, respectively.

The coefficient c gives an over-the-grid summation of the mean escape measure weighting in the two aforementioned aspects. While α_i reinforces the dependence on the ensemble, β_i filters the system's fast dynamics. We also note that $c \leq 1$, where $c = 1$ in the improbable event

that all the orbits visit the same boxes with the same escape time. The higher the value of the escape complexity is, the more complex are the paths made by the orbits before leaving the system.

In practice, due to the time limitation T_{max} , only a subset $\tilde{U} \subseteq U$ composed of M^e initial conditions leads to trajectories that escape from the system. Therefore, since only escape orbits should contribute, we restrict the calculation of the escape complexity coefficient to \tilde{U} and we use

$$\tilde{\alpha}_i = \frac{m_i^e}{M^e} \quad \text{and} \quad \tilde{\beta}_i = \frac{\tau_i^e}{T_{max}} \quad (11)$$

in Eq. (9) instead of α_i and β_i . Here, m_i^e is the number of escape orbits that pass through box B_i with initial condition in \tilde{U} and τ_i^e is the longest escape time between these orbits. If all orbits that begin in the ensemble U escape, then $\tilde{T}^e = T^e$ and Eq. (11) reduces to Eq. (10).

III. ESCAPE ANALYSIS

In this section, we apply our concepts to investigate escape behavior, i.e., the transient behavior of the escape orbits, in two Hamiltonian physical systems: a tokamak equipped with a single-null poloidal divertor and the planar version of the Earth-Moon system.

For the tokamak system, the escape orbits are related to the magnetic field lines that cross the poloidal divertor plate, carrying along impurities and unwanted particles, consequently enhancing the tokamak performance. For the Earth-Moon system, escape orbits are the trajectories of small objects, such as artificial satellites and asteroids, which leave the Moon's realm of gravitational influence towards the Earth's vicinity.

For both systems, our defined grid does not cover the whole phase space, but rather a region V which we are interested in. We, therefore, restrict our analysis to this region and consider only the time spent inside the grid to calculate the escape measure, Eq. (2). Furthermore, in order to deal with the practical limit on integration time, we choose T_{max} as to guarantee that, at least, 85% of the orbits in an ensemble escape, i.e., $M^e \geq 0.85M$. By setting T_{max} and M^e large enough, we also assure that the calculated escape complexity coefficient, Eq. (9), is comparable between the different cases analyzed.

It is also important to note that the definitions presented in Sec. II are based on grids formed by boxes with congruent sides. Therefore, in order to cover the phase space of both systems with the same number of boxes, we normalize them to the unity square $[0, 1] \times [0, 1]$ when carrying out the numerical calculations. One can show that the phase space normalization does not interfere with the results obtained from Eqs. (1)-(9). In particular, when calculating the escape correlation dimension, Eq. (7), the scaling changes the *linear* coefficient of the $\ln I_2^e \times \ln \varepsilon$ graph, but not the *angular* coefficient given by D_2^e .

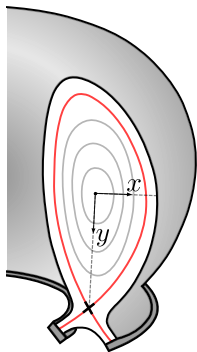


FIG. 1. Poloidal section of a divertor tokamak, showing the closed magnetic field lines (light gray lines), magnetic separatrix (red line), magnetic saddle (black cross) and the rectangular coordinates (x, y) .

A. Single-null divertor tokamak

Poloidal divertors are external magnetic coils that can be assembled in a tokamak to conduct the magnetic field lines at the plasma edge towards an exit point [12]. Technically, the divertor induces a magnetic configuration with a single saddle point (x-point), known as the magnetic saddle, near the divertor plate. Due to perturbations on the magnetic configuration, a chaotic layer is formed around the x-point, allowing the magnetic field lines to escape this chaotic region, passing through the divertor plate [13]. Fig. 1 presents the system's schematic.

The symplectic map proposed in [14] is a phenomenological model for this system and is given by

$$\begin{aligned} x_{n+1} &= x_n - ky_n(1 - y_n), \\ y_{n+1} &= y_n + kx_{n+1}, \end{aligned} \quad (12)$$

where (x_n, y_n) are rectangular coordinates over a poloidal section surface, as depicted in Fig. 1, and the control parameter k is related to the amplitude of toroidal asymmetries that perturb the magnetic field configuration. Here, we use $k = 0.6$, which is adequate to simulate the diverted magnetic field configuration for large tokamaks like ITER [15].

The left panel of Fig. 2 shows the system's phase space x - y . The hyperbolic x-point is located at $(x = 0, y = 1)$ and we consider that a magnetic field line escapes when it crosses the divertor plate, i.e., the escape condition is given by $y > 1$. We are interested in a sub-region V which contains the x-point and is close to the escape threshold. The phase space in V is presented in the right panel of Fig. 2. We observe that the system possess a separatrix chaotic layer embedded with several island chains.

For our numerical simulations, we choose four ensembles inside V and we evolve them up until $T_{max} = 2 \times 10^5$ iterations. Each ensemble is composed of $M = 10^4$ initial conditions and is formed by a square of side-length 1.5×10^{-5} . Then, in order to illustrate the different paths

taken by the orbits in this system, we define a 512×512 grid and we calculate the mean escape measure profile for all cases. The results are shown in Fig. 3.

Since the phase space in V is dominated by a complex configuration of island chains, it is reasonable that we place such ensembles on top of the unstable periodic orbits (UPOs) related to these islands. Sets 1 to 4 are then centered at UPOs of period 28, 57, 30 and 29, which are located at $(0.0, 0.9971)$, $(0.0, 0.9974)$, $(0.0006, 0.9979)$ and $(0.0, 0.9984)$, respectively. We readily observe that the ν_i profile in this region, as depicted by the logarithmic color scale, is highly dependent on the ensemble position as each set leads to different escape behaviors. In especial, it highlights the stickiness experienced by the orbits which begin in sets 1 and 2.

In all cases, the color gradient depicts interesting structures formed between the island chains. These are actually invariant manifolds in the system, which are followed by the orbits as the discrete dynamics evolves [16]. We also notice the low values of the mean escape measure in the neighborhood of the islands, being especially visible for set 4. This phenomenon is related to invariant manifolds as well or, specifically, to the distribution of heteroclinic crossings in the phase space [5].

To statistically investigate the mean escape measure profiles, we present both the histogram and the cumulative histogram for all four different sets in Fig. 4. Here, we consider only the boxes visited at least once by the simulated dynamics. We quickly recognize that not only the histogram distributions, but also the cumulative curves are quite different between the analyzed sets. Set 1 shows a wider distribution in ν_i , presenting at least four distinct peaks. Meanwhile, sets 2, 3 and 4 show more centralized distributions, displaying a different number of peaks in each case, with the last one being the most well behaved.

The calculated histogram distributions stress the different escape behaviors which can emerge from the complex dynamical scenario of the system, as seen in Fig. 3. All orbits beginning in set 1 pass through all the island chains, along their invariant manifolds, before reaching the divertor plate at $y = 1$. Set 4, by its turn, is located closer to the system's exit and the influence from the islands below it is low. Hence, the importance of the island chains regarding the paths followed by the escape orbits depends on the location of the chosen ensemble, which is translated as the number of peaks in Figs. 4.

In order to quantify the differences illustrated by the mean escape measure profiles, we proceed with the calculation of the escape correlation dimension for each analyzed case. In Fig. 5, we plot I_2^e , Eq. (8), as a function of the box side-length ε . We see that all cases can be well fitted by a linear regression in the log-log plot, which corroborates Eq. (7). Also, by comparing the calculated values for D_2^e to the profiles in Fig. 3, we find that the escape correlation dimension is well suited for characterizing the escape behavior in this system. As expected from Fig. 4, these dimensions monotonically decrease as the set of ini-

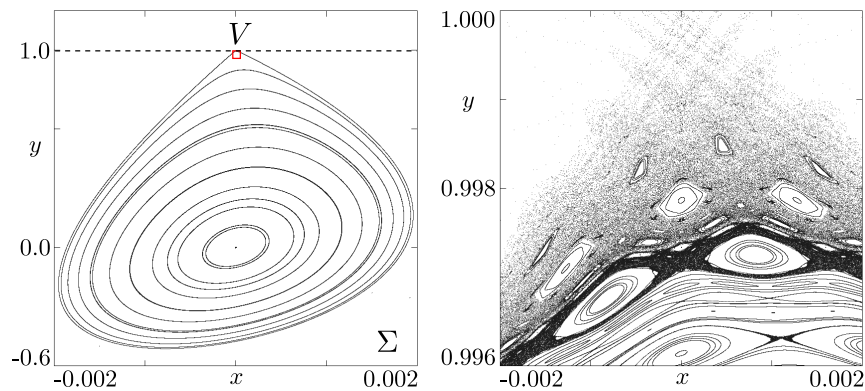


FIG. 2. Phase space x - y of the single-null tokamak map. (Left) Full phase space, denoted as Σ , where the dashed line marks the escape threshold. (Right) Zoom-in on the V region.

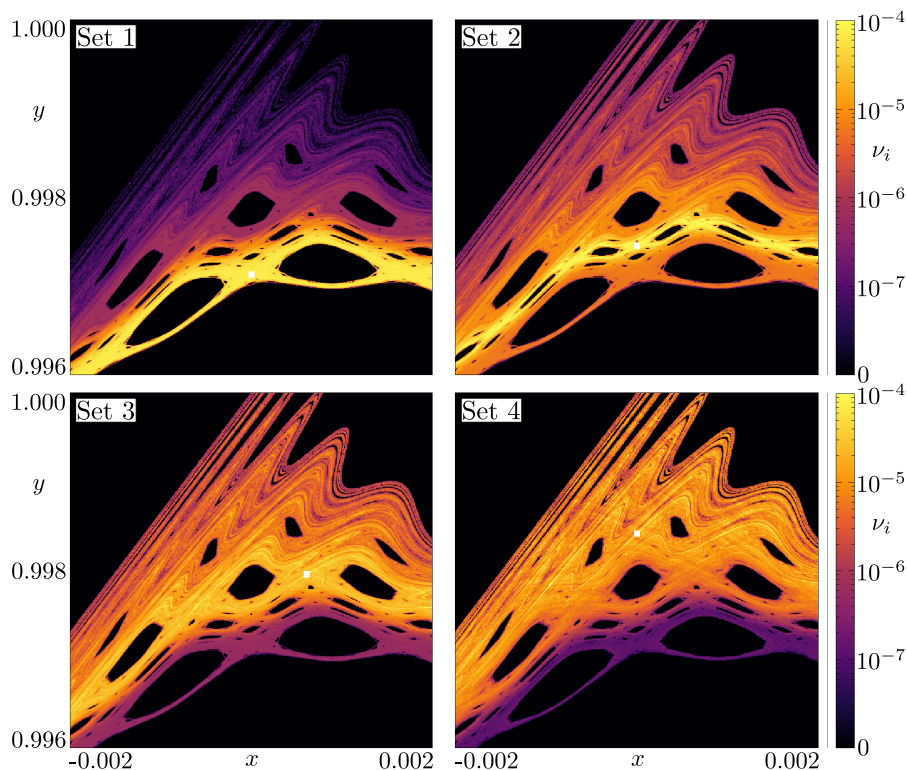


FIG. 3. Profile of the mean escape measure ν_i in logarithmic scale for the single-null tokamak divertor map, calculated on a 512×512 grid in the region V of phase space x - y . The ensembles of initial conditions are represented by the small white squares which are not in scale.

tial conditions gets closer to the escape threshold, which indicates that the escape behavior is more complex when the orbits begin far from the exit.

We continue our analysis by considering a special case, where we choose an ensemble S positioned in the neighborhood of a stability region. Specifically, S is centered at an UPO of period 464 related to the satellite islands of the center island chain of period 30. As the other cases, it is composed of $M = 10^4$ initial conditions and we also iterate it until $T_{max} = 2 \times 10^5$, but, this time, it is formed

by a smaller square of side-length 3×10^{-6} . The mean escape measure profile for this special case is presented in Fig. 6 for a 512×512 grid. We consider the same region V of the phase space that was used for the other ensembles and also a smaller region which focus on the center island (inset). It is clear that the ν_i profiles highlight the presence of stickiness and are able to outline the invariant manifolds associated with the main UPO in each region.

As a second quantitative comparison for the single-null

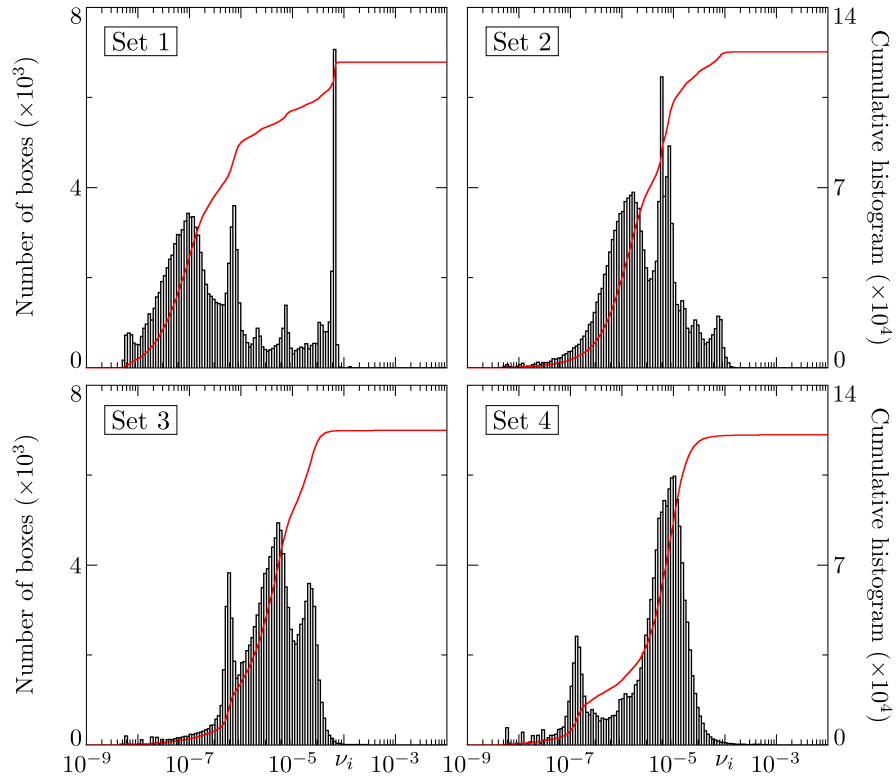


FIG. 4. Histogram (black rectangles) and cumulative histogram (red line) of the mean escape measure ν_i for the single-null tokamak divertor map. The grid is formed by $512^2 = 26.2144 \times 10^4$ boxes and only the ones visited by an orbit were considered.

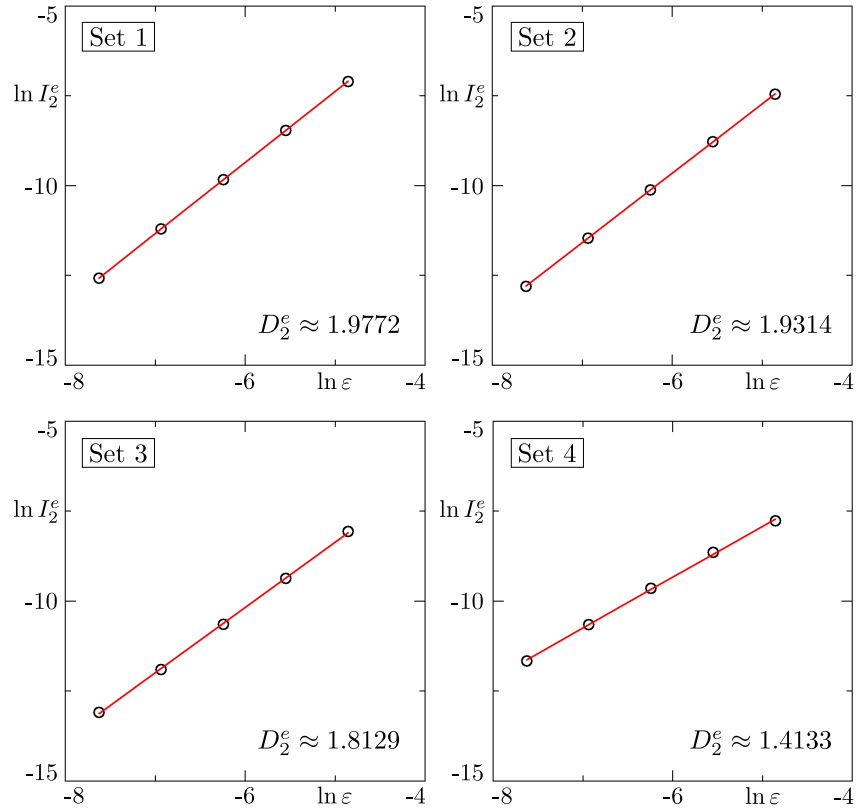


FIG. 5. Linear fitting of $\ln I_2^\epsilon$ as a function of $\ln \epsilon$ for the single null tokamak divertor map. D_2^ϵ is the angular coefficient. The values of the box side-length are $\epsilon = 1/128, 1/256, 1/512, 1/1024$ and $1/2048$ for a phase space normalized to the unity square.

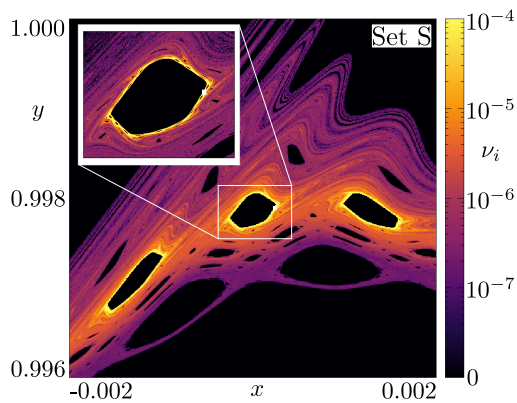


FIG. 6. Profile of the mean escape measure in logarithmic scale for the special case in the single null tokamak divertor map. On the inset, the same profile calculated on a smaller region. The ensemble position is represented by a small white square in both figures.

TABLE I. Escape complexity coefficient c for the analyzed cases in the single-null tokamak divertor map.

Ensemble	Coefficient c
1	2.964×10^{-1}
2	1.099×10^{-1}
3	1.489×10^{-2}
4	3.528×10^{-3}
S	7.058×10^{-1}

tokamak divertor map, we present the computed escape complexity coefficients in Tab. I, considering all the chosen ensembles of initial conditions, including the special one. We readily see that c can properly differentiate between the escape behaviors observed in Figs. 3 and 6. For sets 1 to 4, the values of c decrease as the ensemble location gets closer to the escape boundary. Moreover, for the special set S, the calculated coefficient accurately expresses how complex, in average, it is the path of an escape orbit in this case.

B. Planar Earth-Moon system

The motion of small bodies in the Earth-Moon system can be modeled, as a first approximation, by the planar circular restricted three-body problem. This model concerns the dynamics of a body with negligible mass under the influence of a two-body gravitational potential [17]. In a non-inertial reference frame, which rotates with the same constant frequency as the two-body system, the dimensionless equations of motion on the plane x - y for the third body are given by

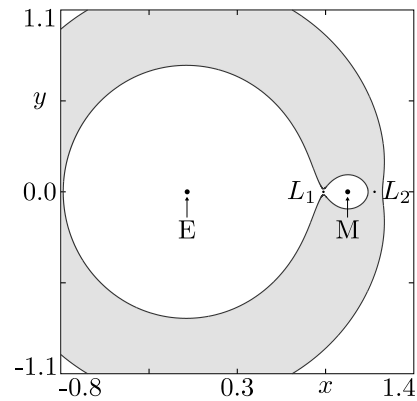


FIG. 7. The Earth-Moon system as modeled by the planar circular restricted three-body problem. The gray area indicates the forbidden region to which the third particle do not have access for $C = 3.187$. Orbits in the vicinity of the Moon can only escape the Moon's realm through the neck in L_1 .

$$\begin{aligned} \ddot{x} - 2\dot{y} &= \frac{\partial \Omega}{\partial x}, \\ \ddot{y} + 2\dot{x} &= \frac{\partial \Omega}{\partial y}, \end{aligned} \quad (13)$$

with

$$\Omega = \frac{1}{2}(x^2 + y^2) + \frac{1-\mu}{r_E} + \frac{\mu}{r_M}, \quad (14)$$

where $\mu = 1.215 \times 10^{-2}$, the ratio between the mass of the Moon and the system's total mass. Also, r_E and r_M are the distances from the primaries, Earth and Moon, which are located at $P_E = (-\mu, 0)$ and $P_M = (1 - \mu, 0)$. The system's schematic is shown in Fig. 7.

From Eq. (13), we can derive the Jacobi constant of motion $C = 2\Omega - \dot{x}^2 - \dot{y}^2$. It restricts the dynamics of the system to a three-dimensional surface and also delimits the accessible region in coordinate space x - y . Next to the Moon and collinear to the primaries, there are two Lagrangian equilibrium points called L_1 and L_2 . If we set the Jacobi constant between the values of C for these points, namely, $C_{L_1} \approx 3.188$ and $C_{L_2} \approx 3.172$, we arrive at a situation where orbits that start near the Moon can transfer to the Earth's vicinity but cannot leave the system.

In this work, we set $C = 3.187$ and we consider that orbits escape when they exit the Moon's realm and enter the Earth's one, which are separated by L_1 . Therefore, the escape condition is given by $x < x_{L_1}$. The equations of motion are numerically integrated up to $T_{max} = 5 \times 10^3$ using the explicit embedded Runge-Kutta Prince-Dormand 8(9) method [18] and orbits are analyzed on a surface of section Σ defined by

$$\Sigma = \{(x, y, \dot{x}, \dot{y}) \mid x_{L_1} < x < x_{L_2}, y = 0, \dot{y} > 0\}, \quad (15)$$

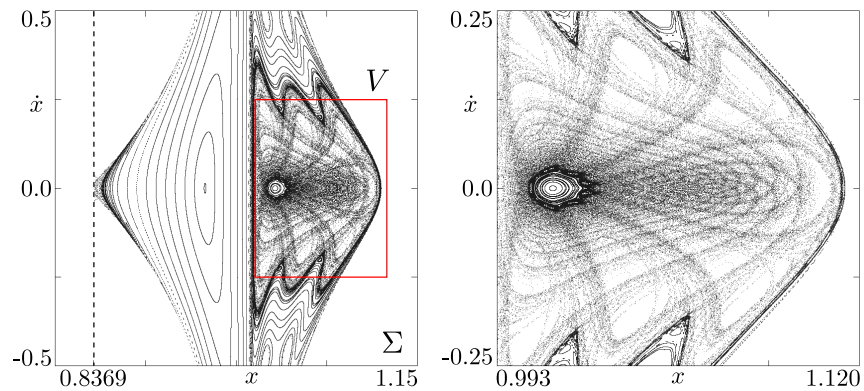


FIG. 8. Phase space $x-\dot{x}$ for the planar Earth-Moon system calculated at the surface of section Σ . (Left) Full phase space, where the dashed line marks the escape threshold. (Right) Zoom-in on our region of interest V .

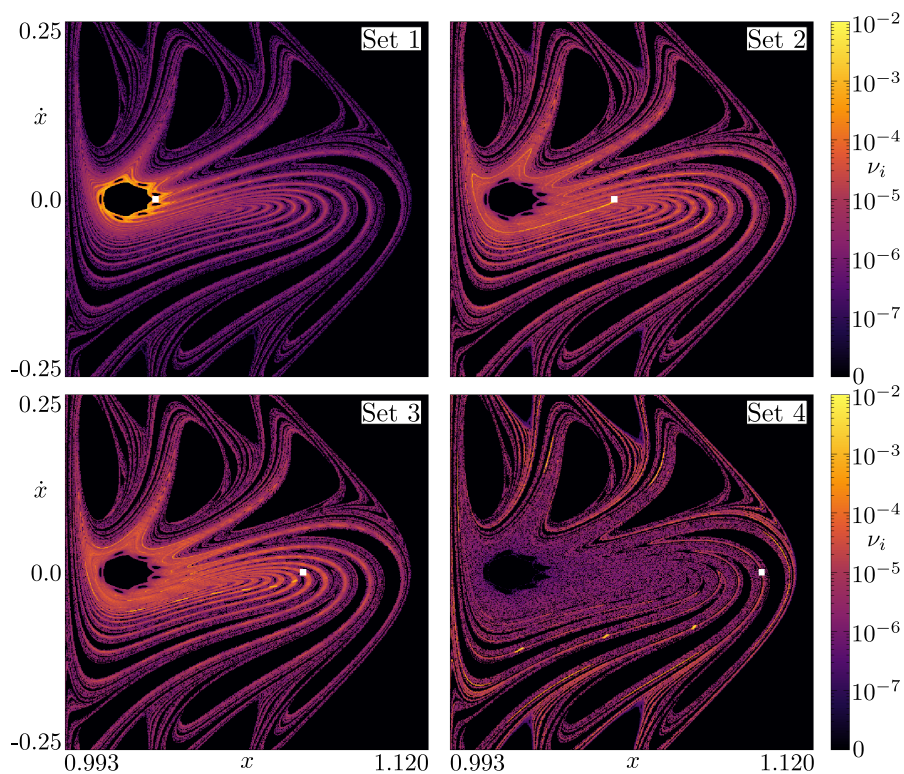


FIG. 9. Profile of the mean escape measure ν_i in logarithmic scale for the Earth-Moon system, calculated on a 512×512 grid in the region V of phase space $x-\dot{x}$. The ensembles of initial conditions are chosen in the surface of section Σ and are represented by the small white squares, which are not in scale.

where $x_{L_1} \approx 0.8369$ and $x_{L_2} \approx 1.1556$ are the positions on the x -axis of L_1 and L_2 , respectively.

Fig. 8 presents the system's phase space $x-\dot{x}$ in our surface of section Σ along with the escape threshold $x = x_{L_1}$ and the region $V \subset \Sigma$ that we are interested in. We can observe one main stability region formed by regular solutions together with a large chaotic sea. There is a clear presence of stickiness around the stability region and areas with higher and lower density of orbits in the chaotic sea.

In order to investigate this system, we choose our four ensembles of $M = 10^4$ initial conditions in the region V . These ensembles are now formed by rectangles of size 5×10^{-4} by 4×10^{-3} in the phase space $x-\dot{x}$ and are equally distant from each other, with set 1 centered at approximately $(1.025, 0.0)$ and set 4 at $(1.102, 0.0)$. In Fig. 9, we present the respective mean escape measure profiles for a grid of 512×512 boxes.

Set 1 is chosen in the neighborhood of the stability region, as we did for the special set in the tokamak system.

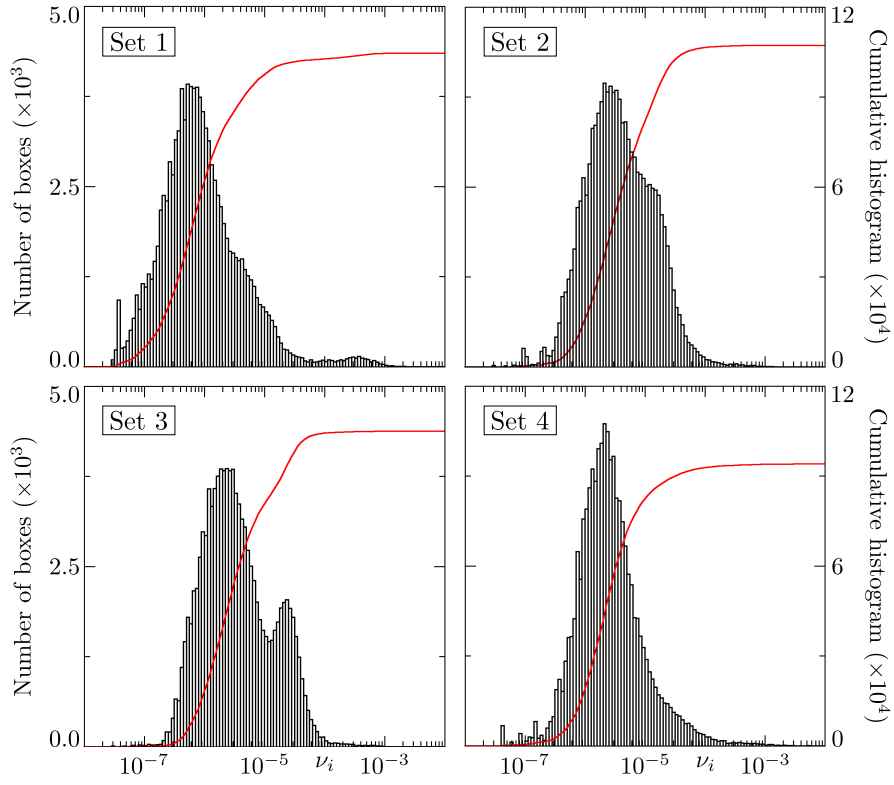


FIG. 10. Histogram (black rectangles) and cumulative histogram (red line) of the mean escape measure ν_i for the Earth-Moon system. The grid is formed by $512^2 = 26.2144 \times 10^4$ boxes and only the ones visited by an orbit were considered.

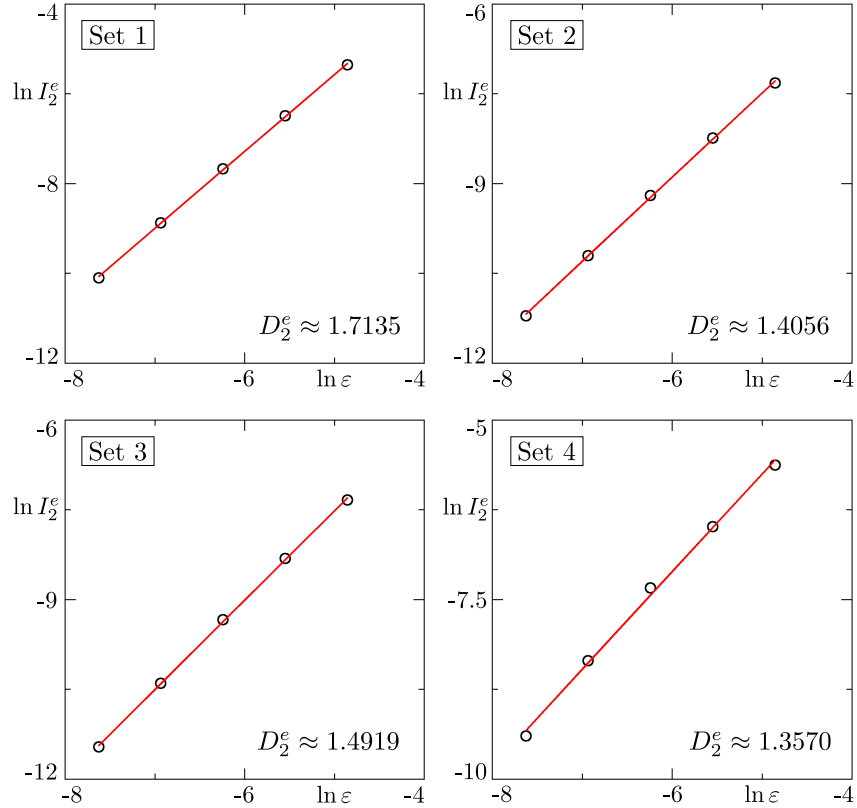


FIG. 11. Linear fitting of $\ln I_2^\varepsilon$ as a function of $\ln \varepsilon$ for the Earth-Moon system, where D_2^ε is the angular coefficient. The values of the box side-lengths are $\varepsilon = 1/128, 1/256, 1/512, 1/1024$ and $1/2048$ for a phase space normalized to the unity square.

In this system, however, we do not have a series of island chains, but rather a main stability region along with a large chaotic sea. As was the case there, we readily notice the higher visitation in the boxes around the stability region, highlighting the stickiness effect and also delineating the invariant manifolds associated with the period-7 UPO in which the set is centered. It is interesting to observe, though, that none of the other cases experience the same stickiness effect. While the orbits that begin in sets 2 and 3 spread across the region V with a higher visitation in the middle section, the ones that begin in set 4 seem to concentrate more on the outer part. Therefore, we observe here three very distinct escape behaviors.

In Fig. 10, we present both the histogram and the cumulative histogram of the mean escape measure for all cases, considering only the visited boxes. As expected due to the stickiness effect, ensemble 1 leads to the highest number of boxes with high mean escape measures, visible as a small bump in the first histogram. Furthermore, even though sets 2 and 3 look similar in Fig. 9, they present different distributions, with the latter having two clear peaks. This could indicate the presence of another UPO in the system, which would be influencing the path of these orbits. As for set 4, the distribution is thinner than the others and the reason why this is so is addressed later.

As before, we initially quantify our observations by calculating the escape correlation dimension for all cases. In Fig. 11, we show I_2^ε as a function of the box side-length ε along the linear fitting for each case and the corresponding value for D_2^ε . The results obtained again validate Eq. (7) and show that such quantity is well suited for characterizing the escape behavior in this system as well. The calculated dimension is higher for set 1 and lower for set 4, as we would expect by looking at Fig. 9. In here, however, the relation between escape correlation dimension and distance from the escape threshold is not linear, since D_2^ε is slightly higher for set 3 when comparing to set 2, which suggests a more complicated escape scenario for this system.

There are two observations we need to make about the interpolation for set 4. First, the total number of visited boxes is significantly lower than the other cases, which is the main information we can extract from the cumulative histograms in Fig. 10. Second, there is a lower number of orbits with high ν_i , as we can also see from the histograms. Therefore, the statistics necessary for calculating I_2^ε and, consequently, the escape dimension correlation is not optimal in this case.

Another information we obtain from the cumulative histograms is that less than half of the grid boxes are visited in all cases. From Fig. 9, we observe the presence of “black lakes”, which are not visited in any of the analyzed cases and yet are not composed by regular structures, since the only region of stability for our parameters is located next to ensemble 1. As special cases, then, we choose two ensembles of initial conditions inside one of these regions and calculate the respective

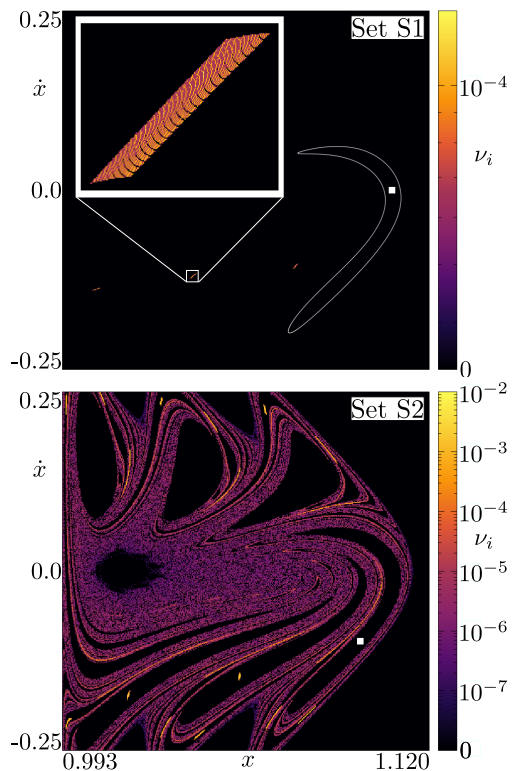


FIG. 12. Profile of the mean escape measure in logarithmic scale for the special cases in the Earth-Moon system. The ensembles are represented out of scale by the white squares. For S1, we also show the contour of the chosen black lake in white and the magnification of the profile for the second crossing.

mean escape measure profiles. The results are presented in Fig. 12, with ensemble S1 centered at $(1.107, 0.0)$ and S2 at $(1.096, -0.09744)$, approximately.

For set S1, we observe an interesting situation where all orbits evolve closely together and exit the system after crossing V three times, which means that there are fast escape routes inside these regions. However, for set S2, the orbits do not rapidly escape, instead they spread across the phase space after crossing V through other black lakes. This means that it is possible for orbits that begin inside these regions to access the same part of phase space as the previous cases, though the opposite is not true as we can see from Fig. 9.

The black lakes are actually formed by the unstable manifolds associated to the Lyapunov orbit, an UPO which revolves around the equilibrium point L_1 . These structures are two-dimensional surfaces and are responsible for the transport of orbits that enter the Moon’s realm [19, 20]. Set S1, particularly, is inside an intersection between manifolds of different stabilities, which causes the orbits that begin in this set to exit the Moon’s vicinity following the stable one [21]. Furthermore, set 4 is partially inside an intersection and, consequently, a portion of the orbits originating in this set rapidly escape

TABLE II. Escape complexity coefficient c for the analyzed cases in the planar Earth-Moon system.

Ensemble	Coefficient c
1	1.718×10^{-1}
2	1.569×10^{-3}
3	2.377×10^{-3}
4	9.460×10^{-4}
S1	4.483×10^{-5}
S2	1.235×10^{-3}

the system, lowering the number of visited boxes, as seen in the histograms of Fig. 10.

We now proceed to the calculation of the escape complexity coefficient, Eq. (9), which is shown in Tab. II for all the cases analyzed in this system, including the two special ones. For cases 1 to 4, Fig. 9, the coefficient c differentiates the escape behavior between the ensembles similarly to the escape correlation dimension, with the value for set 3 being higher than for set 2. For set S1, Fig. 12, the escape complexity coefficient takes into consideration the system's fast dynamics and correctly gives a value lower than the regular cases. Furthermore, c is more adequate than D_2^c for set 4 as well, since it does not depend on the number of visited boxes for statistical purposes.

IV. CONCLUSIONS

In this work, we introduced the mean escape measure, an useful concept to illustrate the transient behavior of escape orbits before exiting the system. We applied such measure to investigate the dynamics of two physical systems with very different dynamical scenarios: a tokamak with a single-null divertor and the planar Earth-Moon system. The first one was described by a two-dimensional map, which presented a complex structure of island chains and associated unstable periodic orbits of varied periods. The second one was modeled by a four-dimensional time-continuous system with a constant of

motion and presented a phase space structure composed by one main regular region along with a large chaotic sea.

By plotting the mean escape measure profiles for these systems, we showed that, depending on the location of the ensemble of initial conditions, the escape orbits described very different paths in the phase space before reaching the exit route. Furthermore, the profiles provided information such as the presence of stickiness in the system and the spatial disposition of invariant manifolds. Later, with the mean escape measure histograms, we were able to highlight the differences between the phase space distribution associated with each ensemble and also between the two physical systems.

The transient dynamical scenarios were quantified by two distinct parameters, the escape correlation dimension and the escape complexity coefficient, both of which were capable of determining which situations lead to the most complex behaviors. The escape correlation dimension is defined directly from the mean escape measure, without further considerations. Additionally, it is independent of the box size, which makes this quantity somewhat more general. However, the computational costs for calculating it were high and it needed a good statistics on box visitation. The escape complexity coefficient, by its turn, takes into consideration how many orbits from the ensemble goes through a given box of the grid and how fast are they. These dynamical aspects are then weighted in the mean escape measure over-the-grid summation. Furthermore, it returned numerical values on a non-linear scale, which makes it easier to differentiate between the analyzed cases. The downside comes from this quantity being associated to a specific box size, which has to be properly chosen.

In summary, we showed that the mean escape measure is an effective novel tool for visually describing the different transient dynamical scenarios that may arise in open Hamiltonian systems.

ACKNOWLEDGMENTS

This study was financed in part by the Coordenação de Aperfeiçoamento de Pessoal de Nível Superior - Brasil (CAPES) - Finance Code 001 and the São Paulo Research Foundation (FAPESP, Brazil), under Grants No. 2018/03211-6 and 2018/03000-5.

-
- [1] A. J. Lichtenberg and M. A. Leiberman, *Regular and chaotic dynamics*, Applied mathematical sciences (Springer-Verlag, 1992).
 - [2] L. Devaney and R. Devaney, *An Introduction To Chaotic Dynamical Systems, Second Edition*, Addison-Wesley advanced book program (Avalon Publishing, 1989).
 - [3] G. M. Zaslavsky, *Chaos in Dynamic Systems* (Harwood Academic Publishers, 1985).
 - [4] G. Contopoulos and M. Harsoula, Stickiness effects in

- chaos, *Celestial Mechanics and Dynamical Astronomy* **107**, 77 (2010).
- [5] V. M. de Oliveira, D. Ciro, and I. L. Caldas, Dynamical trapping in the area-preserving Hénon map, *The European Physical Journal Special Topics* **229**, 1507 (2020).
- [6] S. Bleher, C. Grebogi, E. Ott, and R. Brown, Fractal boundaries for exit in hamiltonian dynamics, *Physical Review A* **38**, 930 (1988).
- [7] S. S. Abdullaev, *Magnetic Stochasticity in Magnetically*

Confined Fusion Plasmas (Springer, 2014).

- [8] V. G. Szebehely, *Theory of orbits, the restricted problem of three bodies* (Academic Press, 1967).
- [9] Y.-C. Lai and T. Tél, *Transient chaos: complex dynamics on finite time scales*, Vol. 173 (Springer Science & Business Media, 2011).
- [10] E. Ott, *Chaos in Dynamical Systems* (Cambridge University Press, 2002).
- [11] P. Grassberger and I. Procaccia, Characterization of strange attractors, *Physical review letters* **50**, 346 (1983).
- [12] A tokamak is a toroidal shaped device which uses a strong magnetic field in order to confine a hot fusion plasma.
- [13] T. Kroetz, M. Roberto, I. L. Caldas, R. L. Viana, and P. J. Morrison, Divertor map with freedom of geometry and safety factor profile, *Plasma Physics and Controlled Fusion* **54** (2012).
- [14] A. Punjabi, A. Verma, and A. Boozer, Stochastic broadening of the separatrix of a tokamak divertor, *Phys. Rev. Lett.* **69** (1992).
- [15] A. Punjabi, H. Ali, and A. Boozer, Symmetric simple map for a single-null divertor tokamak, *Phys. Plasmas* **4** (1996).
- [16] D. Ciro, I. L. Caldas, R. L. Viana, and T. E. Evans, Efficient manifolds tracing for planar maps, *Chaos: An Interdisciplinary Journal of Nonlinear Science* **28**, 093106 (2018).
- [17] C. D. Murray and S. F. Dermott, *Solar System Dynamics* (Cambridge University Press, 1999).
- [18] M. Galassi, B. Gough, F. Rossi, J. Theiler, G. Jungman, M. Booth, and J. Davies, *GNU Scientific Library: Reference Manual* (Network Theory Limited, 2001).
- [19] A. M. O. De Almeida, N. De Leon, M. A. Mehta, and C. C. Marston, Geometry and dynamics of stable and unstable cylinders in hamiltonian systems, *Physica D: Nonlinear Phenomena* **46**, 265 (1990).
- [20] E. Perozzi and S. Ferraz-Mello, *Space Manifold Dynamics: Novel Spaceways for Science and Exploration* (Springer New York, 2010).
- [21] V. M. de Oliveira, P. A. Sousa-Silva, and I. L. Caldas, Order-chaos-order and invariant manifolds in the bounded planar Earth-Moon system (2020), [arXiv:2006.13111](https://arxiv.org/abs/2006.13111) [[nlin.CD](https://arxiv.org/abs/2006.13111)].